International Journal of Energetic Materials and Chemical Propulsion, 14 (6): 519–547 (2015)

VIBRATIONAL AND THERMODYNAMIC PROPERTIES OF 1,3,5-TRIAMINO-2,4,6-TRINITROBENZENE (TATB): COMPARISON OF EXCHANGE-CORRELATION FUNCTIONALS IN DENSITY FUNCTIONAL THEORY

Zhongqing Wu,[1,2] Weiwei Mou,[1] Rajiv K. Kalia,[1] Aiichiro Nakano,[1] & Priya Vashishta[1,*]

[1] *Collaboratory for Advanced Computing and Simulations, Department of Chemical Engineering and Materials Science, Department of Physics and Astronomy, and Department of Computer Science, University of Southern California, Los Angeles, California 90089-0242, USA*

[2] *School of Earth and Space Sciences, University of Science and Technology of China, Hefei, Anhui 230026, China*

[*] Address all correspondence to: Priya Vashishta, E-mail: priyav@usc.edu

Vibrational and thermodynamic properties of TATB have been investigated within the quasiharmonic approximation and density functional theory using three exchange-correlation functionals: local density approximation (LDA), generalized gradient approximation (GGA), and GGA with an empirical van der Waals correction (GGA + vdW). We find that GGA provides a reasonable description of only the heat capacity and thermal expansion, while it fails to reproduce the experimental bulk modulus and volume. Van der Waals correction improves the lattice constants, volume, and bulk modulus, but it fails badly in describing thermal expansion and heat capacity. In contrast, LDA accurately describes all the thermodynamic properties of TATB considered here. For example, the equilibrium volume calculated with LDA is only 4.6% smaller than the experimental value after including vibrational contributions. It is therefore essential to include phonon contributions when comparing the calculated volume with experimental data at ambient conditions. We show that an accurate equation of state of TATB is obtained by simply multiplying the volume calculated with LDA by a factor of 1.046, because LDA predicts the bulk modulus well in the entire pressure range. Therefore, LDA is a satisfactory exchange-correlation functional for TATB because only LDA correctly predicts the volume dependence of vibrational frequencies. All calculations exhibit an abrupt change of the compressibility at a critical pressure, $P_c \sim 0.5$–1.0 GPa. Below P_c, the volume reduction by pressure is mainly due to the lattice contraction along the c axis, whereas above P_c the lattice contracts significantly along all three axes.

KEY WORDS: *TATB, Vibrational and thermodynamic properties, DFT Simulations*

2150–766X/15/$35.00

1. INTRODUCTION

1,3,5-Triamino-2,4,6-trinitrobenzene (TATB) is an important molecular crystal widely used in high-performance energetic applications. Its remarkable stability under thermal, impact, and shock-initiation conditions (Dobratz, 1995; Travis, 1992), as well as its nonlinear optical properties (Ledoux et al., 1990; Son et al., 1999; VoigtMartin et al., 1996; VoigtMartin et al., 1997), have stimulated numerous studies (Makashir and Kurian, 1996; Becuwe and Delclos, 1993; Osmont et al., 2007; Agrawal, 2005; Boddu et al., 2010; Bourasseau et al., 2011; Boyer and Kuo, 2007; Budzevich et al., 2010; Byrd and Rice, 2007; Cady and Larson, 1965; De Lucia et al., 2003; Deopura and Gupta, 1971; Dobratz, 1995; Fedorov and Zhuravlev, 2014; Fell et al., 1998; Filippini and Gavezzotti, 1994; Fried and Ruggiero, 1994; Grebenkin and Kutepov, 2000; Huang et al., 2014; Kolb and Rizzo, 1979; Kroonblawd and Sewell, 2013; Kunz, 1996; Liu et al., 2011; Losada and Chaudhuri, 2009, 2010; Lurnan et al., 2007; Chevalier et al., 1993; Talawar et al., 2006; Mang and Hjelm, 2013; Margetis et al., 2002; McGrane et al., 2005; McGrane and Shreve, 2003; Olinger and Cady, 1976; Pravica et al., 2009; Price, 1988; Qian et al., 2014; Toghiani et al., 2008; Rosen and Dickinson, 1969; Satija et al., 1991; Sewell, 1997; Shan et al., 2014; Son et al., 1999; Stevens et al., 2008; Willey et al., 2009; Taylor, 2013; Thadhani, 1994; Towns, 1983; Traver, 2010; Vergoten et al., 1985; Wu and Fried, 2000; Yetter et al., 1995; Huang et al., 2005; Zeman, 1993; Zhang et al., 2012a, 2012b, 2009). For example, these studies measured thermodynamic properties such as thermal expansion at ambient pressure (Kolb and Rizzo, 1979) and equation of state at room temperature (Kolb and Rizzo, 1979; Stevens et al., 2008), and vibrational properties such as Raman and infrared spectroscopy (Deopura and Gupta, 1971; Satija et al., 1991; Towns, 1983; Vergoten et al., 1985). Although the stability of TATB is usually attributed to its significant inter- and intramolecular hydrogen bonding (Dobratz, 1995), the underlying atomistic mechanisms are still unclear. Detailed structural, vibrational, and thermodynamic properties are indispensable for understanding the atomistic origin of the unusual properties of TATB crystal.

Extensive theoretical studies on TATB crystal have been conducted using empirical interatomic potentials (Bedrov et al., 2009; Gee et al., 2004; Pastine and Bernecker, 1974; Rai et al., 2008; Sewell, 1996) or electronic-structure calculations (Byrd et al., 2007; Grebenkin and Kutepov, 2000; Kunz, 1996; Liu et al., 2007; Budzevich et al., 2009; Oleynik et al., 2007; Wu and Fried, 2000; Zhu et al., 2009) based on the density functional theory (DFT) and Hartree-Fock method. The interatomic potentials describe the crystal structure and bulk modulus at ambient conditions accurately because their parameters are fitted to reproduce experimental data. Furthermore, these potentials have been shown to predict TATB properties at high pressures and temperatures reasonably well (Bedrov et al., 2009; Gee et al., 2004; Rai et al., 2008). In contrast, nonempirical electronic-structure calculations usually have considerable errors in crystal properties of TATB (Byrd et al., 2007; Liu et al., 2007; Wu et al., 2003) and other molecular crystals (Byrd et al., 2007; Byrd et al., 2004; Conroy et al., 2008a, 2008b; Qiu et al., 2006;

Shimojo et al., 2010; Wu et al., 2011; Zhao and Liu, 2008). For example, the generalized gradient approximation (GGA), which is a commonly used exchange-correlation (xc) functional in DFT calculations, tends to overestimate the equilibrium volume of TATB by 20∼30% (Byrd et al., 2007; Liu et al., 2007), while another popular xc functional, the local density approximation (LDA), underestimates it by 10∼15% (Byrd et al., 2007; Liu et al., 2007; Wu et al., 2003). Such failure of DFT is often ascribed to its inadequacy in describing the dispersion interaction. As a result, there is great interest in improving GGA calculations by incorporating van der Waals (vdW) corrections (Dion et al., 2004; Grimme, 2004; Shimojo et al., 2010; Tkatchenko et al., 2010; Tkatchenko and Scheffler, 2009). Another essential issue is the effect of phonons on the thermodynamic properties of molecular crystals. Although the phonon effect on the equilibrium volume is small (about 1–2%) for crystals with larger bulk moduli (Karki et al., 2000; Li et al., 2007; Mounet and Marzari, 2005; Pavone et al., 1993; Sun et al., 2008; Wentzcovitch et al., 2010; Wu and Wentzcovitch, 2007; Wu et al., 2008; Yu and Wentzcovitch, 2006), this effect can be very large for energetic crystals, which exhibit large thermal expansion.

Recently, we reported a detailed investigation of vibrational and thermodynamic properties of the β-HMX (octahydro-1,3,5,7-tetranitro-1,3,5,7-tetrazocine) crystal with LDA, GGA, and GGA with an empirical van der Waals correction (GGA+vdW) (Matsui et al., 2012). We found that phonons significantly increase the equilibrium volume (by more than 5%). LDA predicts the ambient volume to be only 6% less than the experimental value after including the vibration contribution. Most importantly, LDA accurately predicts other thermodynamic properties such as the bulk modulus, heat capacity, and thermal expansion. In contrast, GGA only predicts the heat capacity and thermal expansion well, and produces large errors in the bulk modulus and volume. Although an empirical vdW correction to GGA was found to improve the volume and bulk modulus, the GGA+vdW calculation fails badly in predicting the thermal expansion and heat capacity. Therefore, contrary to the common belief, LDA is a rather good xc functional for β-HMX. In order to clarify whether these observations also hold for other energetic crystals, here we study the vibrational and thermodynamic properties of the TATB crystal in the framework of DFT with three xc functionals—LDA, GGA, and GGA+vdW—to identify the best functional. The other main purpose of this paper is to provide detailed thermodynamic properties of TATB at high temperatures and pressures based on DFT with the best functional thus identified, which are not available in literature to the best of our knowledge.

2. CALCULATION DETAILS

The calculations are performed using pwscf and phonon programs of the Quantum Espresso software for DFT calculations based on the plane-wave basis and pseudopotentials (Giannozzi et al., 2009). The plane-wave cutoff energy (E_{cut}) of 30 Ry is found sufficient to obtain the converged results. Brillouin-zone summations over electronic

states are performed over a 2 × 2 × 2 (2 points) k mesh with a (1/2, 1/2, 1/2) shift from the origin. The Vanderbilt ultrasoft pseudopotentials are generated for C, N, H, and O (Vanderbilt, 1990). For the exchange-correlation functional, we use LDA (Ceperley and Alder, 1980; Perdew et al., 1981) and GGA by Perdew, Burke, and Ernzerhof (PBE) (Perdew et al., 1996).

Van der Waals correction is included using Grimme's DFT-D2 methodology (Grimme, 2004, 2006). The empirical dispersion correction for the energy is given by

$$E_{disp} = -s_6 \sum_{i<j} \frac{C_{ij}}{R_{ij}^6} f_{damp}(R_{ij}) \tag{1}$$

where C_{ij} and R_{ij} denote the dispersion coefficient and the interatomic distance between the ith and jth atoms, and s_6 is a global scaling factor that only depends on the density functional used. A damping function f_{damp} is introduced to ensure that the dispersion correction is negligible for small R_{ij}.

Structural optimizations, with and without the vdW correction, are achieved using the damped variable cell shape molecular dynamics method (Wentzcovitch, 1991). For each fully optimized structure, dynamical matrices are computed on a 2 × 2 × 2 q (wave vector) mesh based on the density functional perturbation theory (DFPT). The dynamical matrices (Baroni et al., 2001) are modified by incorporating the vdW contribution if the structure has been optimized with the vdW correction. The results are then interpolated in a regular 8 × 8 × 8 q mesh to obtain the vibrational density of states.

The Helmholtz free energy in the quasiharmonic approximation (QHA) is given by

$$F(V,T) = U_0(V) + \frac{1}{2}\sum_{q,j} h\varpi_j(q,V) + k_B T \sum_{q,j} \ln\{1 - \exp[-h\varpi_j(q,V)/k_B T]\} \tag{2}$$

where q is a wave vector in the first Brillouin zone, j is an index of the phonon mode with frequency $\varpi_j(q,V)$, V and T are the volume and temperature of the system, and k_B and h are the Boltzmann and Planck constants. The first, second, and third terms in Eq. (2) are the static internal, zero-point, and vibrational energy contributions, respectively. The calculated Helmholtz free energy versus volume is fitted by the Birch-Murnaghan third-order finite strain equation of states, which in turn is used to derive thermodynamic properties.

3. RESULTS AND DISCUSSION

3.1 Lattice Structure

The structure of the TATB crystal is shown in Fig. 1. The unit cell of TATB is triclinic with space group $P\bar{1}$. Each unit cell has two TATB molecules. TATB crystal is highly anisotropic with planar molecules, whose planes are nearly parallel to the ab plane. The

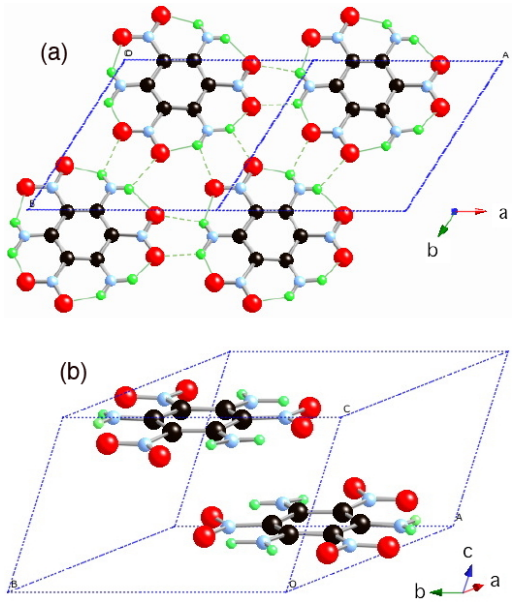

FIG. 1: (a) TATB crystal structure projected along the [001] axis. For clarity of presentation, only the top molecules in the unit cells are shown, namely, for atoms with $0.5 < z < 1.0$, where z is the coefficient for the basic vector along the c lattice vector. Intramolecular and intermolecular hydrogen bonds are displayed with green solid lines and dashed lines, respectively. (b) TATB crystal in the primitive cell. Carbon, nitrogen, oxygen, and hydrogen atoms are shown in black, blue, red, and green, respectively.

interaction between different planes is dominated by vdW interaction, while the intermolecular interaction within the ab plane mainly results from the hydrogen bonds (see green solid and dashed lines in Fig. 1). The anisotropy in TATB structure is clearly reflected in the errors of the lattice parameters by DFT calculations (see Table 1). The errors of a and b are far smaller than those of c for both GGA and LDA. LDA calculations predict a and b quite well but have a significant error in c. GGA calculations show significant errors in all directions but have a dominant error in c. These features on lattice parameters in the LDA and GGA calculation are consistent with previous calculations (Byrd et al., 2007; Liu et al., 2007). In particular, GGA static calculation overestimates the equilibrium volume by 27%, which clearly indicates that GGA is inadequate in treating vdW interaction. (Note that the interaction between different TATB planes along the c axis is dominated by vdW interaction as explained above.) The empirical vdW correction dramatically reduces the errors in the lattice parameters using GGA, which is consistent with previous works (Budzevich et al., 2010; Landerville et al., 2010). The equilibrium volume using GGA+vdW is only 0.9% smaller than the experimental value.

Budzevich et al had indicated anisotropic behavior of TATB under uniaxial compressions (Budzevich et al., 2010). The variations of the lattice parameters of the TATB

TABLE 1: Lattice parameters (a, b, c, α, β, γ), volume (V), and bulk modulus (K_T) of TATB crystal at a pressure of 0 GPa. Both static (without phonon contributions) and QHA calculations within the framework of DFT using LDA, GGA, and GGA+vdW functionals are shown, along with the corresponding experimental data. The numbers in parentheses are deviations from the experimental value in percentage

a **(Å)**	b **(Å)**	c **(Å)**	α **(°)**	β **(°)**	γ **(°)**	V **(Å^3)**	K_T **(GPa)**	
8.864 (–1.6)	8.881 (–1.6)	6.373 (–6.4)	108.67 (0.1)	92.17 (0.4)	120.00 (0.0)	399.6 (–9.6)	19.7	LDA (static)
8.939 (–0.7)	8.954 (–0.8)	6.641 (–2.5)	107.8 (–0.7)	92.08 (0.3)	120.0 (0.0)	422.3 (–4.6)	11.8	LDA (300 K)
9.307 (3.3)	9.324 (3.3)	7.894 (15.9)	105.10 (–3.2)	92.29 (0.5)	120.11 (0.1)	560.1 (26.6)	2.4	GGA (static)
9.346 (3.7)	9.361 (3.7)	8.226 (20.8)	104.30 (–4.0)	92.27 (0.5)	120.14 (0.1)	591.6 (33.7)	1.38	GGA* (300 K)
9.103 (1.0)	9.131 (1.1)	6.634 (–2.6)	109.07 (0.4)	92.11 (0.3)	119.92 (0.0)	438.3 (–0.9)	17.1	GGA+vdW (static)
9.138 (1.4)	9.162 (1.4)	6.740 (–1.0)	108.81 (0.2)	92.06 (0.2)	119.94 (0.0)	449.6 (1.6)	12.86	GGA+vdW (300 K)
9.010	9.028	6.812	108.59	91.82	119.97	442.5	13.6 $\sim$ 16.7 (Olinger and Cady, 1976; Stevens et al., 2008)	Expt. (Olinger and Cady, 1976)

*The effect of zero-point motion to the volume is ignored in order to avoid the extrapolation.

crystal under pressure also exhibit a large anisotropy. LDA, GGA, and GGA+vdW calculations all show the same feature that the anisotropy decreases abruptly at a critical pressure. Results from the GGA calculation are shown in Fig. 2. Note that a and b have nearly identical dependencies on the pressure, which is consistent with previous works (Budzevich et al., 2010). There is a sudden change in the compression ratio of a, b, and c, which is defined as $\Delta a/a$:$\Delta b/b$:$\Delta c/c$, at about 0.5 GPa (Δa, Δb, and Δc are the reduction of a, b, and c, respectively, compared with their zero-pressure values). Below 0.5 GPa, a and b change much more slowly with pressure than c. The compression ratio along the a, b, and c axes is about 1.0:0.94:9.7. The compression in c is one order of magnitude larger than that in a and b. Volume reduction by pressure thus arises mainly from the variation of c at low pressures. Above 0.5 GPa, a and b change much more rapidly with pressure than they do at low pressures. The compression ratio is about 1:1:1.95, which indicates that the variation of a and b also makes a significant contribution to volume reduction at pressures higher than 0.5 GPa. LDA calculation exhibits the same feature, though with a higher critical pressure, $\sim$1.0 GPa. The compression

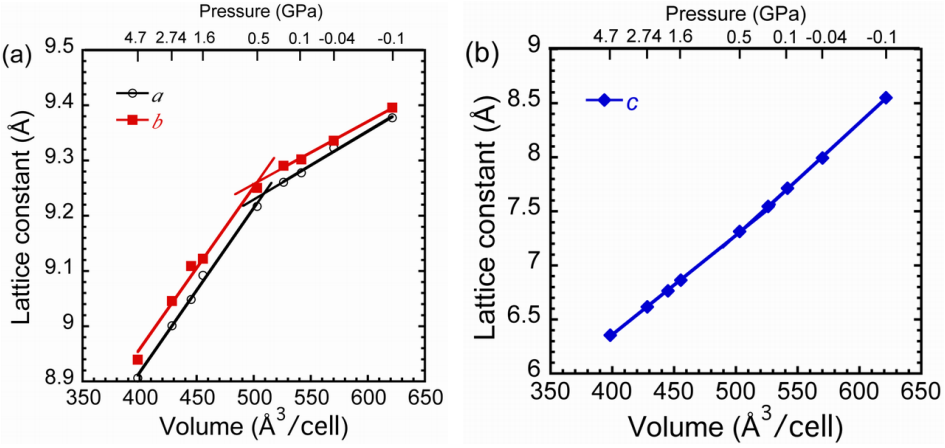

FIG. 2: The variation of (a) lattice constants a and b and (b) the lattice constant c under compression calculated with the GGA.

ratio calculated by LDA is 1:1.04:5.92 and 1:0.99:2.79, respectively, below and above 1.0 GPa.

3.2 Vibrational and Thermodynamic Properties

The vibrational properties of TATB crystal at zero pressure are listed in Table 2 for Raman modes and Table 3 for infrared modes. The dependence of the calculated vibrational properties on the xc functional is similar to that in β-HMX (Matsui et al., 2012). For phonon modes with frequency $>$3000 cm^{-1}, the LDA predicts a smaller frequency than the GGA. But for the other modes except a few, frequencies from the LDA are always larger than those from the GGA. This is consistent with the fact that the LDA predicts the equilibrium volume to be 36% smaller than the GGA. Despite the large volume difference between the LDA and GGA calculations, the corresponding frequency difference is small for modes with frequency $>$1000 cm^{-1}. Both the LDA and GGA results agree well with the experimental data for these modes (Deopura and Gupta, 1971; Satija et al., 1991; Towns, 1983; Vergoten et al., 1985). However, for the modes with frequency $<$300 cm^{-1}, the LDA and GGA results differ significantly, with the LDA results more consistent with the experimental data. The difference between the GGA and GGA+vdW calculations arises from: (1) the reduction of the equilibrium volume at 0 GPa by 28% due to the vdW effect; and (2) the vdW corrections on the force constants. These effects are negligible for high-frequency modes but are significant at low frequencies. The GGA+vdW results are more consistent with the experimental data than the GGA results.

The mode Grüneisen parameter $\gamma_{i,q}$ describes how the phonon frequency depends on the volume and is critical to the computation of thermodynamic properties. It is defined as

TABLE 2: Raman modes of TATB crystal at 0 GPa calculated with the LDA, GGA, and GGA+vdW functionals, along with the experimental data at ambient condition. γ is the mode Grüneisen parameter [see Eq. (3)] at the gamma point, and $\bar{\gamma}$ is the average of the mode Grüneisen parameters in the first Brillouin zone [see Eq. (4)]

Calculation									**Experiment (cm^{-1})**		
LDA			GGA			GGA+vdW			Vergoten et al. (1985)	Deopura and Gupta (1971)	Satija et al. (1991)
ω (cm^{-1})	γ	$\bar{\gamma}$	ω (cm^{-1})	γ	$\bar{\gamma}$	ω (cm^{-1})	γ	$\bar{\gamma}$			
3257.4	0.02	0.02	3374.3	0.01	0.01	3389.5	0.02	0.02	3315		
3253.7	0.01	0.01	3370.8	0	0.01	3386.9	0.02	0.01			
3242.7	0.01	0.01	3362.4	0.01	0.01	3374.9	0.02	0.01			
3167.9	0.02	0.02	3266.6	0.01	0.01	3277.3	0.02	0.02	3215		
3155.6	0.02	0.02	3257.3	0.01	0.01	3269.3	0.03	0.02			
3146.8	0.01	0.01	3251.7	0.01	0.01	3259	0.02	0.01			
1599.6	0.08	0.08	1550.6	0.02	0.03	1562.8	0.09	0.05	1598		
1588.8	0.07	0.08	1544.3	0.02	0.02	1553.2	0.08	0.05			
1578.8	0.06	0.07	1536.7	0.01	0.01	1543	0.07	0.04	1560		
1484.7	0.02	0.03	1483.7	0	0	1497.5	0	0			
1474.7	0	0.02	1480.6	0	0	1489.6	–0.02	–0.01			
1460.5	0.03	0.02	1439.6	0	0	1440.1	0.02	0	1438		
1458.4	0.03	0.01	1438.9	0	0	1439.4	0.02	0.01			
1414.2	0.01	0.01	1394.6	–0.02	0	1394.6	–0.07	–0.02	1413		
1384.2	0.07	0.02	1381	–0.03	–0.01	1378.4	–0.04	–0.02	1372		
1346.1	–0.02	0.04	1339.8	0.02	0.02	1349.8	0.09	0.07			
1327.6	0.05	0.05	1286	0.02	0	1295.1	0.05	0	1315		
1318.2	0.03	0.05	1281.1	0	0	1288.4	0.03	–0.01		1303	

TABLE 2: Continued

Calculation									**Experiment (cm^{-1})**		
LDA			GGA			GGA+vdW			Vergoten et al. (1985)	Deopura and Gupta (1971)	Satija et al. (1991)
ω (cm^{-1})	γ	$\bar{\gamma}$	ω (cm^{-1})	γ	$\bar{\gamma}$	ω (cm^{-1})	γ	$\bar{\gamma}$			
1228.2	0.05	0.04	1203.5	0	0.01	1217.8	0.13	0.03	1212	1229	
1222.8	0.04	0.04	1200.9	0	0.01	1207.2	0.09	0.04			
1221	0.05	0.06	1192.3	0.02	0.03	1196.5	0.04	0.04			
1166	0.03	0.02	1153.2	0	0	1159.1	0.02	0.01	1188		
1154.5	0.01	0.01	1152.7	0	0	1158.3	0.02	0.01	1164	1154	1170
1153	0	0.01	1126.2	0.01	0.02	1130.2	0.08	0.05	1137	1129	
1089.4	–0.08	–0.09	1122.4	–0.04	–0.05	1113.2	–0.09	–0.08			
1030.9	–0.01	–0.01	1027	–0.02	–0.01	1028.8	–0.03	–0.02	1023	1017	1030
1028.7	–0.01	–0.01	1026.6	–0.02	–0.01	1028.7	-0.01	–0.01			
886.7	0.11	0.14	869	–0.02	–0.01	869.1	-0.04	–0.09			890
877.1	0.08	0.10	867.5	–0.03	–0.02	865.6	–0.06	–0.1	878	880	
872.1	0.07	0.13	831.1	0.07	0.04	830.1	0.11	0.07			
864	0.09	0.11	824.7	0.04	0.01	818.8	0.05	0.04			831
855.3	–0.02	0.00	821.4	0.03	0	813.1	0.03	0.01	828		
853.7	0.01	0.02	811.6	0	0	810.3	0.02	0		819	
830.8	0.06	0.12	777.2	0.06	0.02	784	0.15	0.11			
822.8	0.02	0.00	761.3	0.08	0.09	772	0.11	0.05			
802.3	0	0.02	742.1	0.12	0.11	761.1	0.07	0.1			
794.4	–0.02	–0.02	736.7	0	0.01	748.2	0.13	0.02			
757	–0.03	–0.02	734	0.01	0.01	730.5	0	0			

TABLE 2: Continued

Calculation									Experiment (cm^{-1})		
LDA			GGA			GGA+vdW			Vergoten et al. (1985)	Deopura and Gupta (1971)	Satija et al. (1991)
ω (cm^{-1})	γ	$\bar{\gamma}$	ω (cm^{-1})	γ	$\bar{\gamma}$	ω (cm^{-1})	γ	$\bar{\gamma}$			
754.1	–0.04	–0.05	723.6	0.06	0.04	725.2	0.01	0			
714.8	0.03	0.07	696.5	0.01	0.02	698.7	0.03	0.03			
713.4	0.02	0.05	695.9	0	0.01	698.6	0.03	0.03	698		
692.9	–0.04	–0.03	687.4	0	0	693.4	–0.08	–0.06		687	
667.8	–0.06	–0.07	685.8	–0.03	–0.01	688.2	0.02	0			
657.2	–0.01	–0.02	651.5	0	0	650.4	0.01	0			
654	–0.03	–0.05	651.1	0	0	648.2	0	0			
614	0.1	0.15	599	0.03	0.04	607.8	0.11	0.07	609	606	575
523.4	0.11	0.14	502.3	0.06	0.03	512.7	0.15	0.03	513	510	513
522.8	0.12	0.14	501.4	0.05	0.03	512.2	0.14	0.02			
499.9	0.1	0.13	483.2	0.04	0.04	493.1	0.08	0.05			
432.2	0.04	0.03	429.8	0	0.01	442.9	0	–0.03			451
431.7	0.04	0.03	428.5	0.01	0.01	441.8	–0.01	–0.03	447	445	
403	0.25	0.27	375.5	0.07	0.06	392	0.11	0			
383	0.07	0.07	372.7	0.11	0.02	386.7	0.26	0.08	384	381	
370.8	0.29	0.22	349	0.15	0.07	368.8	0.3	0.09			
368.7	0.22	0.2	347.1	0.11	0.03	365	0.22	0.00	362	360	
344.9	0.26	0.24	329.3	0.09	0.04	336.5	0.35	0.19			
341.5	0.21	0.22	328.4	0.08	0.03	333.9	0.27	0.16	324		
299.8	0.24	0.3	281.4	0.05	0.07	290.8	0.24	0.05	291		

TABLE 2: Continued

Calculation									Experiment (cm^{-1})		
LDA			GGA			GGA+vdW			Vergoten et al. (1985)	Deopura and Gupta (1971)	Satija et al. (1991)
ω (cm^{-1})	γ	$\bar{\gamma}$	ω (cm^{-1})	γ	$\bar{\gamma}$	ω (cm^{-1})	γ	$\bar{\gamma}$			
299.6	0.26	0.3	279.7	0.11	0.05	288.9	0.25	0.04			
234.8	0.69	0.71	214.6	0.24	0.11	227.4	0.87	0.44		236	
165.2	3.16	2.95	100.2	1.23	0.32	142.8	4.55	1.27		173	
151	3.37	2.97	93.9	1.22	0.29	141.8	4.75	1.21			
144	2.93	2.77	89.9	1.11	0.23	128.5	4.39	1.04	130		
134.3	2.43	2.75	80.4	2.21	0.39	119.1	3.88	0.99		125	
131.5	2.83	2.75	72.2	2.76	0.39	114.9	4.54	0.96		125	
125.8	2.85	2.89	65.4	2.48	0.45	98.8	4.53	0.93	118		
113.9	2.7	2.86	61	2.55	0.45	92.6	4.63	0.87	96		
93.4	3.49	3.05	48.2	3.31	0.53	81.9	5.07	1.01	88		
68.8	3.43	3.03	32.9	3.15	0.59	69.7	5.57	0.78	80		
57.8	4.46	3.04	18.3	2.42	0.59	62.9	6.07	0.73	57		
46.6	3.76	3.09	–23.1			49.4	6.72	0.65			
37.9	15.1	3.12	–31			33.5	37.78	0.45			

TABLE 3: Infrared modes of TATB crystal at 0 GPa calculated with the LDA, GGA, and GGA+vdW functionals, along with the experimental data at ambient condition. γ is the mode Grüneisen parameter [see Eq. (3)] at the gamma point, and $\bar{\gamma}$ is the average of the mode Grüneisen parameters in the first Brillouin zone [see Eq. (4)]

Calculation									**Experiment (cm^{-1})**		
LDA			GGA			GGA+vdW			Vergoten et al. (1985)	Deopura and Gupta (1971)	Towns (1983)
ω (cm^{-1})	γ	$\bar{\gamma}$	ω (cm^{-1})	γ	$\bar{\gamma}$	ω (cm^{-1})	γ	$\bar{\gamma}$			
3257.1	0.02	0.02	3373.8	0.01	0.01	3389.2	0.03	0.01	3328		
3251.1	0.01	0.01	3370.3	0	0.01	3385.1	0.02	0.01	3327		
3242.4	0.01	0.01	3361.5	0.01	0.01	3374.5	0.02	0.01	3317	3317	
3166.8	0.02	0.02	3267.1	0.01	0.01	3278.3	0.03	0.02	3217		
3155.2	0.02	0.01	3257.5	0.01	0.01	3269.3	0.03	0.02	3214		
3145.3	0.01	0.01	3251.7	0	0.01	3259.7	0.02	0.01			
1594.6	0.08	0.08	1548.2	0.02	0.02	1561	0.09	0.05	1611	1618	1614
1593.7	0.07	0.08	1548	0.02	0.02	1558.1	0.08	0.05	1565	1571	1567
1581.6	0.07	0.07	1538.7	0.01	0.01	1547.6	0.08	0.04	1555	1549	
1473.4	0	0.02	1477.8	0	0	1485.6	–0.02	–0.02			
1464.7	0	0.02	1475.7	–0.01	–0.01	1481.3	–0.03	–0.03			
1462.5	0.02	0.02	1441.2	0	0	1442.6	0.03	0.01	1445	1447	1444
1456.5	0.01	0	1438.1	0	0	1438.2	0.02	0			
1398.5	0.01	0	1394.2	–0.04	–0.01	1391.4	-0.1	–0.04	1404	1416	
1379.8	0.03	0.04	1371.7	–0.03	–0.02	1365.8	–0.03	–0.03			
1356.1	0	0.07	1339.5	0.02	0.03	1349.5	0.09	0.07			
1335.9	0.06	0.06	1289.8	0.02	0.02	1301.6	0.07	0.02	1322	1322	1322
1328.4	0.04	0.05	1286.3	0.02	0.01	1295.6	0.05	0			

TABLE 3: Continued

Calculation									**Experiment (cm^{-1})**		
LDA			GGA			GGA+vdW			Vergoten et al. (1985)	Deopura and Gupta (1971)	Towns (1983)
ω (cm^{-1})	γ	$\bar{\gamma}$	ω (cm^{-1})	γ	$\bar{\gamma}$	ω (cm^{-1})	γ	$\bar{\gamma}$			
1226.5	0.05	0.04	1200.7	0.04	0	1203	0.06	0.03	1229		
1222	0.04	0.03	1198.3	0	0	1198.7	0.04	0.03	1221		
1221.3	0.04	0.06	1196.9	0	0.03	1197.4	0.04	0.04	1219	1216	
1167	0.03	0.02	1155.6	0	0.01	1161.9	0.02	0.03	1173	1177	
1155.7	0.01	0.02	1153.2	0	0.01	1159.2	0.02	0.02			
1152.8	0	0	1126	0.02	0.02	1129.7	0.07	0.04			
1088.8	–0.08	–0.09	1121.2	–0.04	–0.05	1112.2	–0.09	–0.08	1050		
1028.4	–0.02	–0.01	1027.3	–0.02	–0.01	1029.7	–0.02	–0.01	1033		
1026.1	–0.02	–0.01	1026.4	–0.02	–0.01	1028	–0.03	–0.02	1028	1028	
884.7	0.1	0.12	869.8	–0.01	–0.02	870.1	–0.04	–0.08	880	880	
872.9	0.05	0.1	867.8	–0.03	–0.02	865.7	–0.06	–0.1			
867.9	0.07	0.13	829.3	0.06	0.03	826.5	0.1	0.07			
857.6	0.02	0.09	823.1	0.03	0	816.5	0.05	0.02			
854.3	0	0	817.6	0.03	0	811.9	0.06	0.01			
845.3	0.09	0.02	812.1	0	0	810.7	0.01	0	831		
829.3	0.07	0.09	773.3	0.01	0	774.3	0.08	0.09			
818	0.06	0.02	751.9	0.13	0.1	768.1	0.06	0.05			
800	0	0.01	741	0.09	0.09	752.5	0.14	0.1	783	782	782
793	–0.03	–0.02	734.6	0	0	733.6	0.01	0	752		
755	–0.03	–0.03	725.3	0.04	0.02	730.1	0	–0.01	731	730	

TABLE 3: Continued

Calculation									Experiment (cm^{-1})		
LDA			GGA			GGA+vdW			Vergoten et al. (1985)	Deopura and Gupta (1971)	Towns (1983)
ω (cm^{-1})	γ	$\bar{\gamma}$	ω (cm^{-1})	γ	$\bar{\gamma}$	ω (cm^{-1})	γ	$\bar{\gamma}$			
754.8	–0.04	–0.04	720.7	0.05	0.05	723.2	0.03	0.01	725		
714	0.03	0.07	695.8	0.01	0.01	698	0.04	0.02			
713.1	0.03	0.05	695	0.01	0.01	697.3	0.04	0.02	708		
696.2	0	0	686	–0.01	–0.01	693.3	–0.09	–0.08	697	700	
667	–0.07	–0.08	682.2	0	–0.01	683	–0.01	–0.01			
662.2	0.01	–0.01	653.3	0.01	0.01	655.5	0.07	0.03			
655	–0.03	–0.03	650.7	0	0	647.5	–0.01	–0.02			
614.5	0.08	0.16	598.1	0.03	0.04	607	0.11	0.06	606		
523.1	0.11	0.14	502.3	0.05	0.03	513.3	0.14	0.03	567		
521.8	0.1	0.13	501.3	0.05	0.03	511	0.13	0.02	517	510	
499	0.08	0.12	481.6	0.04	0.04	492.3	0.11	0.04			
431.3	0.04	0.02	428.7	0.01	0.01	441.8	–0.02	–0.04	448		
430.9	0.03	0.02	428.1	0.01	0.01	441	–0.03	–0.05	446	445	
403.4	0.25	0.27	376.8	0.07	0.06	393.4	0.15	–0.01			
379.6	0.02	0.05	372.2	0.06	0.02	385.4	0.25	0.07			
367.8	0.18	0.17	348.7	0.13	0.07	367.4	0.24	0.08			
365.7	0.2	0.13	347.3	0.09	0.03	366.6	0.24	0.01	365		
347.6	0.28	0.24	330	0.1	0.05	338.3	0.35	0.2			
342.4	0.19	0.24	329.1	0.08	0.03	334.9	0.25	0.18			
300.2	0.25	0.31	282	0.08	0.07	291.1	0.24	0.05			

TABLE 3: Continued

Calculation									Experiment (cm^{-1})		
LDA			GGA			GGA+vdW			Vergoten et al. (1985)	Deopura and Gupta (1971)	Towns (1983)
ω (cm^{-1})	γ	$\bar{\gamma}$	ω (cm^{-1})	γ	$\bar{\gamma}$	ω (cm^{-1})	γ	$\bar{\gamma}$			
299.3	0.24	0.3	281.3	0.07	0.06	290.2	0.26	0.04	290		
235.6	0.74	0.74	215.2	0.24	0.14	227.4	0.87	0.51			
146.6	3.03	2.8	93.3	0.96	0.25	134.1	4.44	1.08	135		
139.4	2.67	2.82	88.4	1.16	0.31	128.1	4.89	1.03	122		
132.9	2.32	2.72	85.3	1.36	0.31	119.4	4.13	1	114		
114.6	2.1	2.95	70.8	0.88	0.46	108.5	5.25	0.98			
110.3	2.99	2.91	63.2	1.79	0.45	94.3	4.62	0.86			
97.1	3.56	2.96	60.6	2.26	0.51	81.9	5.12	1.14			
92.4	3.25	3.05	38.5	3.1	0.58	76.8	4.9	0.87	86		
73	4.25	3.1	35.5	3.26	0.58	57.3	5.57	0.63	72		
63.6	3.08	3.03	20.3	12.8	0.6	42.7	7.8	0.56	58		

$$\gamma_{i,q} = -\frac{\partial \ln \omega_{i,q}}{\partial \ln V} \tag{3}$$

where i is the mode index and q is the wave vector in the reciprocal space. (Note that there is no thermal expansion within the harmonic approximation because $\gamma_{i,q} = 0$.) The calculated mode Grüneisen parameters in TATB crystal have the same features as those in β-HMX A (Matsui et al., 2012). γ_i values are given in Tables 2 and 3 for $q = 0$ (gamma point), which clearly depend on the mode frequency. For high-frequency modes, γ_i is close to zero because the lengths of strong molecular bonds in the molecular crystal are not sensitive to the volume change. On the contrary, low-frequency modes usually have γ_i values much larger than 1. Tables 2 and 3 also list the integration of γ_i over the first Brillouin zone:

$$\bar{\gamma}_i = \frac{\int \gamma_{i,q} dq}{\int dq} \tag{4}$$

High-frequency modes in some way are like Einstein modes, and their γ_i and $\bar{\gamma}_i$ values are close to each other, since their frequencies are almost independent of wave vector q. For low-frequency modes, LDA and GGA calculations exhibit vastly different behaviors. γ_i and $\bar{\gamma}_i$ calculated by LDA are not much different, which means that the gamma-point ($q = 0$) value γ_i is a good representation of the integration of $\gamma_{i,q}$ over the first Brillouin zone. In contrast, $\bar{\gamma}_i$ is only about $1/4 \sim 1/2$ of γ_i in the GGA calculations. Therefore, thermodynamic properties derived from GGA calculations using only the gamma point are not reliable. The vdW correction increases $\bar{\gamma}_i$ only slightly and does not change the major feature that $\bar{\gamma}_i$ is far smaller than γ_i.

In GGA calculations, we obtain two imaginary modes at gamma point at 0 GPa, whose frequencies appear as negative values in Table 2. At higher pressures, the imaginary modes disappear. The imaginary modes from GGA cause a problem in the calculation of thermodynamic properties using QHA, see Eq. (2). However, both modes are imaginary only for a narrow range of *q* values around the gamma point. The contribution of the imaginary frequencies to the phonon density of states (PDoS) is negligible. Furthermore, these imaginary modes may become stable after including phonon-phonon interactions, since the triclinic TATB is stable at ambient condition. Therefore, it is reasonable to calculate thermodynamic properties of TATB using QHA by ignoring the two imaginary frequencies. Although the proportion of PDoS of the imaginary frequencies to that of all frequencies is very small, it increases with the volume. Consequently, the calculated thermodynamic properties become less reliable above a certain volume. Note that the zero-point motion [second term in Eq. (2)] increases the volume by about 3% but has a small effect on thermodynamic properties. By ignoring this term, we can thus obtain more reliable thermodynamic properties. Accordingly, the volume difference between the static and 300 K GGA calculations arises solely from the temperature contribution; see Table 1.

Thermal expansion of TATB crystal calculated with the LDA, GGA, and GGA + vdW functionals is compared with experimental data in Fig. 3. The GGA and LDA

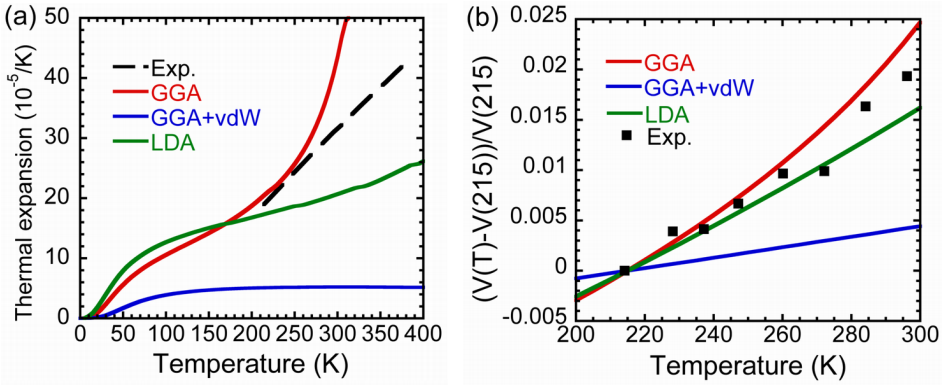

FIG. 3: (a) Thermal expansion of TATB at 0 GPa. Experimental data are obtained by fitting the volume vs temperature data by Kolb and Rizzo (1979). (b) Relative volume variation with temperature, where $V(T)$ is the volume at temperature T. Experimental data are taken from Kolb and Rizzo (1979). Results from the LDA, GGA, and GGA+vdW calculations are shown.

calculations predict nearly the same thermal expansion below 150 K. Above 150 K, the thermal expansion in GGA increases rapidly and exhibits a superlinear behavior, which is likely due to the omission of anharmonic effects in QHA (Matsui et al., 2012). The experimental data in Fig. 3, which are obtained by fitting the measured volume vs temperature data in Kolb and Rizzo (1979) are located between the LDA and GGA results. As mentioned in Sec. III-A, the compression ratio among a, b, and c calculated by GGA is 1:0.94:9.7 below 0.5 GPa. Consequently, the linear coefficient of the thermal expansion of the c axis is almost 10 times that of the b axis according to the constrained QHA (Carrier et al., 2007), which assumes that the lattice parameters only depend on the volume. [This assumption was shown to work well for $MgSiO_3$ (Carrier et al., 2007)]. The result is consistent with the experimental data, which indicate that the relative expansion of the c axis is about 12 times that of the b axis. This suggests that the constrained QHA can also be applied to molecular crystals such as TATB. The LDA calculation predicts that the relative expansion of the c axis is about 6 times that of the b axis, since the compression ratio along a, b, and c from LDA is 1:1.04:5.92 below 1 GPa, which is slightly smaller than the experimental data. Both the LDA and GGA results show that the a and b axes have almost the same linear coefficients of thermal expansion, which does not agree with the Kolb and Rizzo (1979) experimental results that the relative expansion of the b axis is about 3 times of that of the a axis but is consistent with the recent measurement by Sun et al. (2010). The vdW correction makes the thermal expansion of TATB much smaller than the GGA result and worsens the agreement with the experimental data (Kolb and Rizzo, 1979).

Similar to the cases of other energetic molecular crystals such as β-HMX (Matsui et al., 2012), the phonon contribution to the equilibrium volume is remarkably large in

TATB compared to nonmolecular crystals. As shown in Table 1, the equilibrium volume increases about 7% (5%) when phonon effects are included with GGA (LDA). Based on our results on TATB and β-HMX and similarly large thermal expansion of other energetic materials such as RDX (Cady, 1972), PETN (Cady, 1972), and NTO (Bolotina et al., 2003), observed experimentally, we expect that the large vibrational contribution to the volume is a common feature of all energetic molecular crystals. This is in contrast to the most nonmolecular crystals (Li et al., 2007; Mounet and Marzari, 2005; Pavone et al., 1993; Sun et al., 2008; Wentzcovitch et al., 2010; Wu and Wentzcovitch, 2007; Wu et al., 2008; Yu and Wentzcovitch, 2006), where the vibrational contribution to the volume is only 1∼2%. Consequently, the common practice of evaluating the exchange-correlation functional by comparing the static DFT calculation results with room temperature experimental data is problematic for molecular crystals like the energetic materials. The LDA functional is usually not preferred, because it significantly underestimates the volume of most molecular crystals with static calculation. However, when the vibrational effects are included, the discrepancy between the volume predicted by LDA and the experimental value is considerably reduced. For TATB, the discrepancy between LDA and the experimental volume decreases from –9.6% to –4.6% when vibrational effects are included (see Table 1). Therefore, contrary to the common belief, we find that LDA is a good exchange-correlation functional for energetic molecular crystals like TATB and HMX. The equilibrium volume from GGA+vdW increases about 2.5% when phonon effects are included, which is slightly smaller than previous works (Landerville et al., 2010).

The equation of state and bulk modulus of TATB at 300 K calculated with LDA, GGA, and GGA+vdW functionals are compared with experimental data in Fig. 4. Overestimation of the volume by GGA decreases with the pressure. The vdW correction reduces the volume overestimation by GGA (by 32% at 0 GPa and 4% at 10 GPa), and the resulting equation of state with the vdW correction agrees well with the experimental data. This indicates that the bulk modulus with the vdW correction is quite accurate, which is confirmed by the good agreement between the calculated result and the experimental data (Olinger and Cady, 1976; Stevens et al., 2008) at 0 GPa; see Table 4. As shown in Fig. 4(b), the bulk modulus from GGA is much smaller than the experimental data even at high pressures, and the bulk modulus from LDA is almost identical to that from GGA+vdW. This means that the LDA accurately predicts the bulk modulus in the entire pressure range. Thus the error in volume by the LDA calculation is invariant with the pressure. The error in volume from the LDA is 4.6% at 0 GPa (see Table 1). By multiplying the LDA volume by a constant factor of 1.048, we get an equation of state that agrees well with the experimental data in the entire pressure range. This simple recipe for obtaining an accurate equation of state has been shown to work for β-HMX as well, where we obtain a highly accurate equation of state of β-HMX by multiplying the volume from LDA by a constant factor of 1.06. (The LDA error in the volume at ambient condition is 6% for β-HMX.) We expect that this is also true for other energetic

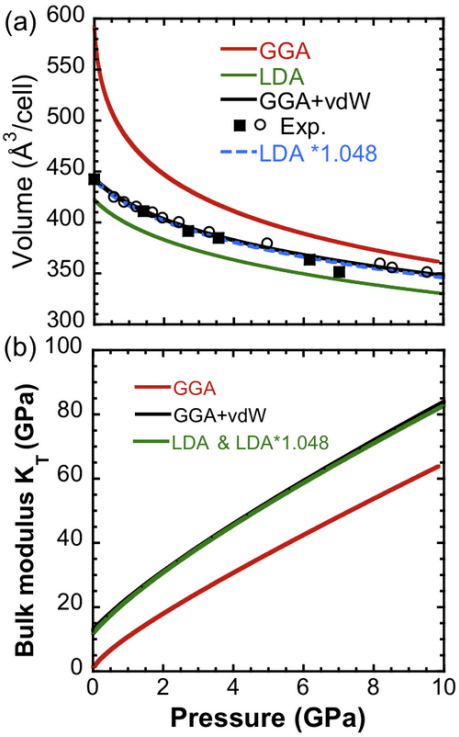

FIG. 4: Pressure dependence of (a) volume and (b) isothermal bulk modulus. Results from the LDA, GGA, and GGA+vdW calculations are compared with the experimental data by Kolb and Rizzo (1979) (solid squares) and Stevens et al. (2008) (open circles).

molecular crystals such as RDX, PETN, and NTO. Thus, an accurate equation of state for an energetic molecular crystal at broad temperature and pressure range can be obtained by multiplying the volume calculated within the LDA by a constant factor (1+*error*), where the *error* is the relative volume difference between the LDA and experimental results at ambient condition. In contrast, the equation of state of energetic molecular crystals from the GGA+vdW method can only apply to the narrow temperature around room temperature because of its significant underestimation of thermal expansion.

As shown in Fig. 5, the LDA also reproduces the experimental heat capacity at constant pressure C_P of TATB very well (Baytos, 1979), as does GGA. However, the vdW correction largely underestimates C_P. Overall, the GGA is good at describing the thermal expansion α and C_P, but fails to describe the isothermal bulk modulus K_T and the equilibrium volume V. On the other hand, GGA+vdW is good at describing K_T and V, but fails for α and C_P. The LDA accurately describes all thermodynamic properties—K_T, C_P, α, V—with a slight underestimation of $V \sim 5\%$), which can be corrected easily by multiplying with a constant factor as mentioned above. Since the thermal Grüneisen parameter γ_{th} is related to these properties through the relation

TABLE 4: Thermodynamic properties of TATB crystal at ambient condition, where α is the thermal expansion, C_P and C_v are the heat capacities at constant pressure and constant volume, respectively, γ_{th} and V are the thermal Grüneisen parameter and the equilibrium volume, and K_T and K'_T are the isothermal bulk modulus and its pressure derivative

α **(10^{-5}/K)**	C_P **(J/mol/K^{-1})**	C_V **(J/mol/K^{-1})**	γ_{th}	V **(Å^3)**	K_T **(GPa)**	K'_T	
20.68	276.60	257.32	1.20	422.3	11.8	12.7	LDA
43.40	274.35	260.44	0.41	591.58	1.38	12.2	GGA
5.22	259.92	289.52	0.35	442.88	12.85	12.9	GGA+ vdW
30.2 Kolb and Rizzo (1979)	280.69 Pastine and Bernecke (1974)			442.9 Olinger and Cady (1976)	13.6 Stevens et al. (2008) 16.7 Olinger and Cady (1976)	12.4 Stevens et al. (2008) 5.7 Olinger and Cady (1976)	Experi- ment

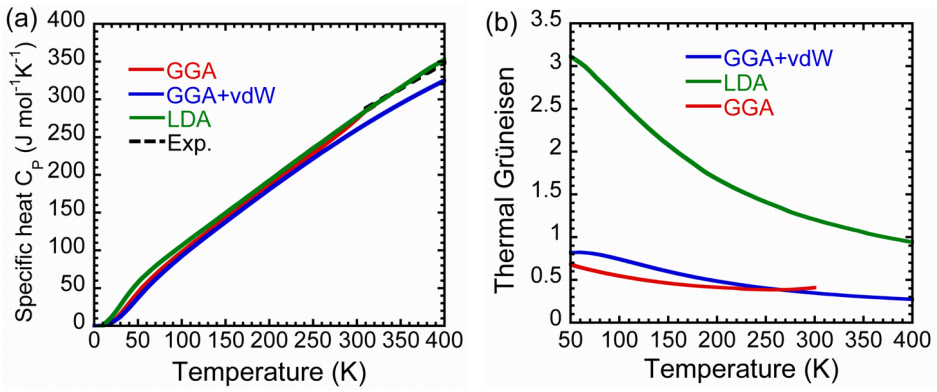

FIG. 5: (a) Heat capacity and (b) thermal Grüneisen parameter at 0 GPa. Results from the LDA, GGA, and GGA+vdW calculations are compared with the experimental data by Pastine and Bernecke (1974).

$$\gamma_{th} = \frac{\alpha V K_T}{C_V} \tag{5}$$

where C_V is the heat capacity at constant volume, γ_{th} estimated with the LDA should be reasonable as well. As shown in Fig. 5, the GGA gives γ_{th} much smaller than the LDA value, and the vdW correction only slightly changes the GGA value. Why γ_{th} from the

GGA is smaller than from the LDA is understood as follows: γ_{th} is a weighted average of the mode Grüneisen parameter $\bar{\gamma}_i$, and at low temperatures, low-frequency modes provide dominant contributions to γ_{th}. As listed in Tables 2 and 3, $\bar{\gamma}_i$ for low-frequency modes calculated with the GGA are significantly smaller than those obtained from the LDA, which makes the GGA estimate of γ_{th} very small. Though the GGA considerably underestimates $\bar{\gamma}_i$, the GGA can still describe α well, because it also underestimates VK_T at the same time to cancel out this error. (K_T is only about a tenth of the experimental value; see Tables 1 and 4.) The vdW correction improves VK_T dramatically but changes $\bar{\gamma}_i$ only slightly. As a result, the vdW correction worsens the α calculated with the GGA. In order to describe thermodynamic properties correctly, the vdW correction must increase $\bar{\gamma}_i$ significantly in the GGA calculation. Note that all dispersion coefficients in the empirical vdW method adopted here are fixed independent of the electron density distribution. In reality, the local electron density varies from atom to atom, and this should affect dispersion coefficients. Although this effect may change the phonon frequency only slightly, it may cause a dramatic change in $\bar{\gamma}_i$, i.e., the volume dependence of the phonon frequency. Some vdW methods (Dion et al., 2004; Tkatchenko and Scheffler, 2009) are being developed to incorporate this effect, which would provide better estimates of all thermodynamic properties.

4. CONCLUSION

We have investigated the effect of the exchange-correlation functional on the vibrational and thermodynamic properties of TATB molecular crystal. Our main finding is that the LDA is a good exchange-correlation functional for predicting these properties. The same conclusion was drawn previously for β-HMX (Matsui et al., 2012). Previous works also indicated that LDA is much better than GGA for graphite and the adsorption of adenine on graphite (Hasegawa and Nishidate, 2004; Ortmann et al., 2005). We thus expect that this is likely to be a common feature among other energetic materials or even among broader molecular crystals.

The GGA describes the thermal expansion coefficient α of TATB and β-HMX (Matsui et al., 2012) quite well, which is remarkable given the fact that the GGA dramatically underestimates their bulk moduli K_T. Our phonon calculations reveal that this is due to a cancellation of errors, i.e., the GGA also underestimates the mode Grüneisen parameters $\bar{\gamma}_i$, resulting in a small thermal Grüneisen parameter γ_{th}. The underestimations in γ_{th} and K_T cancel each other, and thus the GGA predicts α quite well. The empirical vdW correction resolves the underestimation of K_T by the GGA but only slightly increases γ_{th}, making α from the GGA+vdW too small. When compared with the GGA and GGA+vdW, the LDA satisfactorily describes all thermodynamic properties, including α, K_T, C_P, and γ_{th}.

Because molecular crystals like TATB and β-HMX (Matsui et al., 2012) have similar γ_{th} and much smaller K_T compared with other types of crystals, α of molecular

crystals are usually several times larger than that of nonmolecular crystals. Accordingly, the volume of a molecular crystal changes significantly with temperature. Therefore, for molecular crystals, it is essential to include phonon contributions to the volume when evaluating the quality of the exchange-correlation functional. The GGA calculations, which already overestimate the volume of TATB by 27% in static calculations, become worse after including phonon contributions. In contrast, the LDA results become much better after including phonon contributions, with the volume deviation from the experimental value of only 4.6% at room temperature. Furthermore, the error in volume from the LDA does not change with pressure, since the LDA accurately predicts the bulk modulus of TATB over a wide range of pressure. Consequently, we can simply obtain a highly accurate equation of state of TATB from the LDA calculations.

ACKNOWLEDGMENTS

This research is supported by the Office of Naval Research, Air Warfare and Weapons Department, through Grant No. N00014-12-1-0555. Computations were performed at the University of Southern California High Performance Computing Center using the 150 teraflops Linux cluster and the 4,096-processor Linux cluster at the Collaboratory for Advanced Computing and Simulations.

REFERENCES

Agrawal, J. P., Some new high energy materials and their formulations for specialized applications, *Propellants Explos. Pyrotech*., vol. **30**, pp. 316–328, 2005.

Baroni, S., de Gironcoli, S., Dal Corso, A., and Giannozzi, P., Phonons and related crystal properties from density-functional perturbation theory, *Rev. Mod. Phys*., vol. **73**, pp. 515–562, 2001.

Baytos, J. F., Specific heat and thermal conductivity of explosives, mixtures, and plastic-bonded explosives determined experimentally, Report No. LA-8034-MS, Los Alamos Scientific Laboratory, 1979.

Becuwe, A. and Delclos, A., Low-sensitivity explosives for low-vulnerability warheads, *Propellants Explos. Pyrotech*., vol. **18**, pp. 1–10, 1993.

Bedrov, D., Borodin, O., Smith, G. D., Sewell, T. D., Dattelbaum, D. M., and Stevens, L. L., A molecular dynamics simulation study of crystalline 1,3,5-triamino-2,4,6-trinitrobenzene as a function of pressure and temperature, *J. Chem. Phys*., vol. **131**, p. 224703, 2009.

Boddu, V. M., Viswanath, D. S., Ghosh, T. K., and Damavarapu, R., 2,4,6-triamino-1,3,5-trinitrobenzene (TATB) and TATB-based formulations—A review, *J. Hazard. Mater*., vol. **181**, pp. 1–8, 2010.

Bolotina, N. B., Zhurova, E. A., and Pinkerton, A. A., Energetic materials: Variable-temperature crystal structure of beta-NTO, *J. Appl. Crystallogr*., vol. **36**, pp. 280–285, 2003.

Bourasseau, E., Maillet, J., Desbiens, N., and Stoltz, G., Microscopic calculations of Hugoniot curves of neat triaminotrinitrobenzene (TATB) and of its detonation products, *J. Phys. Chem. A*, vol. **115**, no. 39, pp. 10729–10737, 2011.

Boyer, E. and Kuo, K. K., Modeling of nitromethane flame structure and burning behavior, *Proc. Combust. Inst*., vol. **31**, pp. 2045–2053, 2007.

Budzevich, M., Conroy, M., Landerville, A., Lin, Y., Oleynik, I., and White, C. T., Hydrostatic equation of state and anisotropic constitutive relationships in 1,3,5-triamino-2,4,6-trinitrobenzene (TATB), *Shock Compression of Condensed Matter 2009*: *Proceedings of the Conf. of the American Physical Society Topical Group on Shock Compression of Condensed Matter*, vol. **1195**, p. 545, Nashville, TN, June 28–July 3, 2009.

Budzevich, M., Landerville, A., Conroy, M., Lin, Y., Oleynik, I., and White, C., Hydrostatic and uniaxial compression studies of 1,3,5-triamino-2,4,6-trinitrobenzene using density functional theory with Van der Waals correction, *J. Appl. Phys*., vol. **107**, p. 113524, 2010.

Byrd, E. F. C., Scuseria, G. E., and Chabalowski, C. F., An ab-initio study of solid nitromethane, HMX, RDX, and CL20: Successes and failures of DFT, *J. Phys. Chem. B*, vol. **108**, pp. 13100–13106, 2004.

Byrd, E. F. C. and Rice, B. M., Ab-initio study of compressed 1,3,5,7-tetranitro-1,3,5,7-tetraazacyclooctane (HMX), cyclotrimethylenetrinitramine (RDX), 2,4,6,8,10,12-hexanitrohexaazaisowurzitane (CL-20), 2,4,6-trinitro-1,3,5-benzenetriamine (TATB), and pentaerythritol tetranitrate (PETN), *J. Phys. Chem. C*, vol. **111**, pp. 2787–2796, 2007.

Byrd, E. F. C., Chabalowski, C. F., and Rice, B. M., An ab-initio study of nitromethane, HMX, RDX, CL-20, PETN, and TATB, *Theory Pract. Energetic Mater*., vol. **vii**, pp. 696–700, 923, 2007.

Cady, H. H., Coefficient of thermal expansion of pentaerythritol tetranitrate and hexahydro-1,3,5-trinitro-s-triazine (RDX), *J. Chem. Eng. Data*, vol. **17**, p. 369, 1972.

Cady, H. H. and Larson, A. C., Crystal structure of 1,3,5-triamino-2,4,6-trinitrobenzene, *Acta Crystallogr*., vol. **18**, p. 485, 1965.

Carrier, P., Wentzcovitch, R., and Tsuchiya, J., First-principles prediction of crystal structures at high temperatures using the quasiharmonic approximation, *Phys. Rev. B: Condens. Matter*, vol. **76**, p. 064116, 2007.

Ceperley, D. M. and Alder, B. J., Ground state of the electron-gas by a stochastic method, *Phys. Rev. Lett*., vol. **45**, pp. 566–569, 1980.

Chevalier, M., Carion, N., Protat, J. C., and Redasse, J. C., Propagation phenomena on the detonation wave front, *Phys. Rev. Lett*., vol. **71**, pp. 712–714, 1993.

Conroy, M. W., Oleynik, I. I., Zybin, S. V., and White, C. T., First-principles investigation of anisotropic constitutive relationships in pentaerythritol tetranitrate, *Phys. Rev. B*: *Condens. Matter*, vol. **77**, p. 094107, 2008a.

Conroy, M. W., Oleynik, I. I., Zybin, S. V., and White, C. T., First-principles anisotropic constitutive relationships in beta-cyclotetramethylene tetranitramine (beta-HMX), *J. Appl. Phys*., vol. **104**, p. 053506, 2008b.

De Lucia, F. C., Harmon, R. S., McNesby, K. L., Winkel, R. J., and Miziolek, A. W., Laser-induced breakdown spectroscopy analysis of energetic materials, *Appl. Optics*, vol. **42**, pp. 6148–6152, 2003.

Deopura, B. L. and Gupta, V. D., Vibration spectra of 1,3,5-triamino-2,4,6-trinitrobenzene, *J. Chem. Phys*., vol. **54**, p. 4013, 1971.

Dion, M., Rydberg, H., Schroder, E., Langreth, D. C., and Lundqvist, B. I., Van der Waals density functional for general geometries, *Phys. Rev. Lett*., vol. **92**, p. 246401, 2004.

Dobratz, B. M., The insensitive high explosive triaminotrinitrobenzene TATB: Development and characterization—1888 to 1994, Report no. LA-13014-H, Los Alamos National Lab., NM, 1995.

Fedorov, I. A. and Zhuravlev, Y. N., Hydrostatic pressure effects on structural and electronic properties of TATB from first principles calculations, *Chem. Phys*., vol. **436**, pp. 1–7, 2014.

Fell, N. F., Vanderhoff, J. A., Pesce-Rodriguez, R. A., and McNesby, K. L., Characterization of Raman spectral changes in energetic materials and propellants during heating, *J. Raman Spectrosc*., vol. **29**, pp. 165–172, 1998.

Filippini, G. and Gavezzotti, A., The crystal-structure of 1,3,5-triamino-2,4,6-trinitrobenzene - centrosymmetric or noncentrosymmetric, *Chem. Phys. Lett*., vol. **231**, pp. 86–92, 1994.

Fried, L. E. and Ruggiero, A. G., Energy-transfer rates in primary, secondary, and insensitive explosives, *J. Phys. Chem*., vol. **98**, pp. 9786–9791, 1994.

Gee, R. H., Roszak, S., Balasubramanian, K., and Fried, L. E., Ab initio based force field and molecular dynamics simulations of crystalline TATB, *J. Chem. Phys*., vol. **120**, pp. 7059–7066, 2004.

Giannozzi, P., Baroni, S., Bonini, N., Calandra, M., Car, R., Cavazzoni, C., Ceresoli, D., Chiarotti, G. L., Cococcioni, M., Dabo, I., Dal Corso, A., de Gironcoli, S., Fabris, S., Fratesi, G., Gebauer, R., Gerstmann, U., Gougoussis, C., Kokalj, A., Lazzeri, M., Martin-Samos, L., Marzari, N., Mauri, F., Mazzarello, R., Paolini, S., Pasquarello, A., Paulatto, L., Sbraccia, C., Scandolo, S., Sclauzero, G., Seitsonen, A. P., Smogunov, A., Umari, P., and Wentzcovitch, R. M., Quantum espresso: A modular and open-source software project for quantum simulations of materials, *J. Phys.: Condens. Matter*, vol. **21**, p. 395502, 2009.

Grebenkin, K. F. and Kutepov, A. L., Band gap estimation for a triaminotrinitrobenzene molecular crystal by the density-functional method, *Semiconductors*, vol. **34**, pp. 1161–1162, 2000.

Grimme, S., Accurate description of Van der Waals complexes by density functional theory including empirical corrections, *J. Comput. Chem*., vol. **25**, pp. 1463–1473, 2004.

Grimme, S., Semiempirical GGA-type density functional constructed with a long-range dispersion correction, *J. Comput. Chem*., vol. **27**, pp. 1787–1799, 2006.

Hasegawa, M. and Nishidate, K., Semiempirical approach to the energetics of interlayer binding in graphite, *Phys. Rev. B: Condens. Matter*, vol. **70**, p. 205431, 2004.

Huang, Z., Chen, B., and Gao, G., IR vibrational assignments for TATB from the density functional B3LYP/6-31G(d) method, *J. Mol. Struct*., vol. **752**, pp. 87–92, 2005.

Huang, B., Hao, X. F., Zhang, H. B., Yang, Z. J., Ma, Z. G., Li, H. Z., Nie, F. D., and Huang, H., Ultrasonic approach to the synthesis of HMX@TATB core-shell microparticles with improved mechanical sensitivity, *Ultrason. Sonochem*., vol. **21**, pp. 1349–1357, 2014.

Kakar, S., Nelson, A. J., Treusch, R., Heske, C., van Buuren, T., Jimenez, I., Pagoria, P., and Terminello, L. J., Electronic structure of the energetic material 1,3,5-triamino-2,4,6-trinitrobenzene, *Phys. Rev. B: Condens. Matter*, vol. **62**, pp. 15666–15672, 2000.

Karki, B. B., Wentzcovitch, R. M., de Gironcoli, S., and Baroni, S., High-pressure lattice dynamics and thermoelasticity of MgO, *Phys. Rev. B: Condens. Matter*, vol. **61**, pp. 8793–8800,

2000.

Kolb, J. R. and Rizzo, H. F., Growth of 1,3,5-triamino-2,4,6-trinitrobenzene (TATB), 1. Anisotropic thermal-expansion, *Propellants Explos. Pyrotech*., vol. **4**, pp. 10–16, 1979.

Kroonblawd, M. P. and Sewell, T. D., Theoretical determination of anisotropic thermal conductivity for crystalline 1,3,5-triamino-2,4,6-trinitrobenzene (TATB), *J. Chem. Phys*., vol. **139**, p. 074503, 2013.

Kunz, A. B., Ab-initio investigation of the structure and electronic properties of the energetic solids TATB and RDX, *Phys. Rev. B: Condens. Matter*, vol. **53**, pp. 9733–9738, 1996.

Landerville, A. C., Conroy, M. W., Budzevich, M. M., Lin, Y., White, C. T., and Oleynik, I. I., Equations of state for energetic materials from density functional theory with Van der Waals, thermal, and zero-point energy corrections, *Appl. Phys. Lett*., vol. **97**, p. 251908, 2010.

Ledoux, I., Zyss, J., Siegel, J. S., Brienne, J., and Lehn, J. M., 2nd-harmonic generation from nondipolar noncentrosymmetric aromatic charge-transfer molecules, *Chem. Phys. Lett*., vol. **172**, pp. 440–444, 1990.

Li, L., Wentzcovitch, R. M., Weidner, D. J., and Da Silva, C. R. S., Vibrational and thermodynamic properties of forsterite at mantle conditions, *J. Geophys. Res*., vol. **112**, no. B05206, 2007.

Liu, H., Zhao, J. J., Du, J. G., Gong, Z. Z., Ji, G. F., and Wei, D. Q., High-pressure behavior of TATB crystal by density functional theory, *Phys. Lett. A*, vol. **367**, pp. 383–388, 2007.

Liu, L., Liu, Y., Zybin, S., Sun, H., and Goddard, W., ReaxFF-lg: Correction of the ReaxFF reactive force field for London dispersion, with applications to the equations of state for energetic materials, *J. Phys. Chem. A*, vol. **115**, pp. 11016–11022, 2011.

Losada, M. and Chaudhuri, S., Theoretical study of elementary steps in the reactions between aluminum and teflon fragments under combustive environments, *J. Phys. Chem. A*, vol. **113**, pp. 5933–5941, 2009.

Losada, M. and Chaudhuri, S., Finite size effects on aluminum/teflon reaction channels under combustive environment: A Rice-Ramsperger-Kassel-Marcus and transition state theory study of fluorination, *J. Chem. Phys*., vol. **133**, p. 134305, 2010.

Lurnan, J. R., Wehrman, B., Kuo, K. K., Yetter, R. A., Masoud, N. M., Manning, T. G., Harris, L. E., and Bruck, H. A., Development and characterization of high performance solid propellants containing nano-sized energetic ingredients, *Proc. Combust. Inst*., vol. **31**, pp. 2089–2096, 2007.

Makashir, P. S. and Kurian, E. M., Spectroscopic and thermal studies on the decomposition of 2,4,6-triamino-1,3,5-trinitrobenzene, *J. Therm. Anal. Calorim*., vol. **46**, pp. 225–236, 1996.

Mang, J. T. and Hjelm, R. P., Fractal networks of inter-granular voids in pressed TATB, *Propellants Explos. Pyrotech*., vol. **38**, pp. 831–840, 2013.

Margetis, D., Kaxiras, E., Elstner, M., Frauenheim, T., and Manaa, M. R., Electronic structure of solid nitromethane: Effects of high pressure and molecular vacancies, *J. Chem. Phys*., vol. **117**, pp. 788–799, 2002.

Matsui, M., Ito, E., Yamazaki, D., Yoshino, T., Guo, X. Z., Shan, S. M., Higo, Y., and Funakoshi, K. I., Static compression of (Mg-0.83, Fe-0.17)O and (Mg-0.75, Fe-0.25)O ferropericlase up to 58 GPa at 300, 700, and 1100 K, *Am. Mineral*, vol. **97**, pp. 176–183, 2012.

McGrane, S., Barber, J., and Quenneville, J., Anharmonic vibrational properties of explosives from temperature-dependent Raman, *J. Phys. Chem. A*, vol. **109**, pp. 9919–9927, 2005.

McGrane, S. D. and Shreve, A. P., Temperature-dependent Raman spectra of triaminotrinitrobenzene: Anharmonic mode couplings in an energetic material, *J. Chem. Phys*., vol. **119**, pp. 5834–5841, 2003.

Mounet, N. and Marzari, N., First-principles determination of the structural, vibrational and thermodynamic properties of diamond, graphite, and derivatives, *Phys. Rev. B*, vol. **71**, p. 205214, 2005.

Oleynik, I. I., Conroy, M., and White, C. T., Anisotropic constitutive relationships in energetic materials: Nitromethane and RDX, in *APS Topical Conference on Shock Compression of Condensed Matter—2007*, Parts 1 and 2, vol. **955**, pp. 401–404, American Institute of Physics, Melville, NY, 2007.

Olinger, B. and Cady, H. H., The hydrostatic compression of explosives and detonation products to 10 GPa (100 kbars) and their calculated shock compression: Results for PETN, TATB, CO_2, and H_2O, *The 6th Intl. Symposium on Detonation*, San Diego, CA, p. 700, August 24–27, 1976.

Ortmann, F., Schmidt, W. G., and Bechstedt, F., Attracted by long-range electron correlation: Adenine on graphite, *Phys. Rev. Lett*., vol. **95**, p. 186101, 2005.

Osmont, A., Catoire, L., Gkalp, I., and Yang, V., Ab-initio quantum chemical predictions of enthalpies of formation, heat capacities, and entropies of gas-phase energetic compounds, *Combust. Flame*, pp. 262–273, 2007.

Pastine, D. J. and Bernecker, R. R., P,V,E,T equation of state for 1,3,5-triamino-2,4,6-trinitrobenzene, *J. Appl. Phys*., vol. **45**, pp. 4458–4468, 1974.

Pavone, P., Karch, K., Schutt, O., Windl, W., Strauch, D., Giannozzi, P., and Baroni, S., Ab-initio lattice-dynamics of diamond, *Phys. Rev. B: Condens. Matter*, vol. **48**, pp. 3156–3163, 1993.

Perdew, J. P., Mcmullen, E. R., and Zunger, A., Density-functional theory of the correlation-energy in atoms and ions—A simple analytic model and a challenge, *Phys. Rev. A: At. Mol. Opt. Phys*., vol. **23**, pp. 2785–2789, 1981.

Perdew, J. P., Burke, K., and Ernzerhof, M., Generalized gradient approximation made simple, *Phys. Rev. Lett*., vol. **77**, pp. 3865–3868, 1996.

Pravica, M., Yulga, B., Tkachev, S., and Liu, Z., High-pressure far- and mid-infrared study of 1,3,5-triamino-2,4,6-trinitrobenzene, *J. Phys. Chem. A*, vol. **113**, pp. 9133–9137, 2009.

Price, D., Effect of particle size on the shock sensitivity of porous HE, *J. Energetic Mater*., vol. **6**, pp. 283–317, 1988.

Qian, W., Zhang, C. Y., Xiong, Y., Zong, H. H., Zhang, W. B., and Shu, Y. J., Thermal expansion of explosive molecular crystals: Anisotropy and molecular stacking, *Cent. Eur. J. Energetic Mater*., vol. **11**, pp. 59–81, 2014.

Qiu, L., Xiao, H. M., Zhu, W. H., Xiao, J. J., and Zhu, W., Ab initio and molecular dynamics studies ofcrystalline TNAD (trans-1,4,5,8-tetranitro-1,4,5,8-tetraazadecalin), *J. Phys. Chem. B*, vol. **110**, pp. 10651–10661, 2006.

Rai, N., Bhatt, D., Siepmann, J. I., and Fried, L. E., Monte Carlo simulations of 1,3,5-triamino-2,4,6-trinitrobenzene (TATB): Pressure and temperature effects for the solid phase and vapor-

liquid phase equilibria, *J. Chem. Phys*., vol. **129**, p. 194510, 2008.

Rosen, J. M. and Dickinson C., Vapor pressures and heats of sublimation of some high melting organic explosives, *J. Chem. Eng. Data*, vol. **14**, p. 120, 1969.

Satija, S. K., Swanson, B., Eckert, J., and Goldstone, J. A., High-pressure Raman-scattering and inelastic neutron-scattering studies of triaminotrinitrobenzene, *J. Phys. Chem*., vol. **95**, pp. 10103–10109, 1991.

Sewell, T. D., Monte Carlo simulations of crystalline TATB, Decomposition, Combustion Detonation Chemistry of Energetic Materials, *Mater. Res. Soc. Symp. Proc*., vol. **418**, pp. 67–72, 1996.

Sewell, T. D., Molecular dynamics and Monte Carlo calculations of the physical properties of RDX, HMX, and TATB, *Proc. of the Conf. of the American Physical Society Shock Compression of Condensed Matter*, vol. **429**, Amherst, Massachusetts, July 27–Aug. 1, p. 269, 1997.

Shan, T. R., van Duin, A. C. T., and Thompson, A. P., Development of a ReaxFF reactive force field for ammonium nitrate and application to shock compression and thermal decomposition, *J. Phys. Chem. A*, vol. **118**, pp. 1469–1478, 2014.

Shimojo, F., Wu, Z. Q., Nakano, A., Kalia, R. K., and Vashishta, P., Density functional study of 1,3,5-trinitro-1,3,5-triazine molecular crystal with Van der Waals interactions, *J. Chem. Phys*., vol. **132**, p. 094106, 2010.

Son, S. F., Asay, B. W., Henson, B. F., Sander, R. K., Ali, A. N., Zielinski, P. M., Phillips, D. S., Schwarz, R. B., and Skidmore, C. B., Dynamic observation of a thermally activated structure change in 1,3,5-triamino-2,4,6-trinitrobenzene (TATB) by second harmonic generation, *J. Phys. Chem. B*, vol. **103**, pp. 5434–5440, 1999.

Stevens, L. L., Velisavljevic, N., Hooks, D. E., and Dattelbaum, D. M., Hydrostatic compression curve for triamino-trinitrobenzene determined to 13.0 GPa with powder x-ray diffraction, *Propellants Explos. Pyrotech*., vol. **33**, pp. 286–295, 2008.

Sun, T., Umemoto, K., Wu, Z. Q., Zheng, J. C., and Wentzcovitch, R. M., Lattice dynamics and thermal equation of state of platinum, *Phys. Rev. B: Condens. Matter*, vol. **78**, p. 024304, 2008.

Sun, J., Kang, B., Xue, C., Liu, Y., Xia, Y. X., Liu, X. F., and Zhang, W., Crystal state of 1,3,5-triamino-2,4,6-trinitrobenzene (TATB) undergoing thermal cycling process, *J. Energetic Mater*., vol. **28**, pp. 189–201, 2010.

Talawar, M. B., Agarwal, A. P., Anniyappan, M., Gore, G. M., Asthana, S. N., and Venugopalan, S., Method for preparation of fine TATB (2–5 μm) and its evaluation in plastic bonded explosive (PBX) formulations, *J. Hazard. Mater. B*, vol. **137**, pp. 1848–1852, 2006.

Taylor, D. E., Intermolecular forces and molecular dynamics simulation of 1,3,5-triamino-2,4,6-trinitrobenzene (TATB) using symmetry adapted perturbation theory, *J. Phys. Chem. A*, vol. **117**, pp. 3507–3520, 2013.

Thadhani, N. N., Shock-induced and shock-assisted solid-state chemical-reactions in powder mixtures, *J. Appl. Phys*., vol. **76**, pp. 2129–2138, 1994.

Tkatchenko, A. and Scheffler, M., Accurate molecular Van der Waals Interactions from ground-state electron density and free-atom reference data, *Phys. Rev. Lett*., vol. **102**, p. 073005, 2009.

Tkatchenko, A., Romaner, L., Hofmann, O. T., Zojer, E., Ambrosch-Draxl, C., and Scheffler, M.,

Van der Waals interactions between organic adsorbates and at organic/inorganic interfaces. *MRS Bull.*, vol. **35**, pp. 435–442, 2010.

Toghiani, R. K., Toghiani, H., Maloney, S. W., and Boddu, V. M., Prediction of physicochemical properties of energetic materials, *Fluid Phase Equilibr.*, vol. **264**, pp. 86–92, 2008.

Towns, T. G., Vibrational-spectrum of 1,3,5-triamino-2,4,6-trinitrobenzene, *Spectrochim. Acta, Part A*, vol. **39**, pp. 801–804, 1983.

Traver, C. M., Corner turning and shock desensitization experiments plus numerical modeling of detonation waves in the triaminotrinitrobenzene based explosive LX-17, *J. Phys. Chem. A*, vol. **114**, pp. 2727–2736, 2010.

Travis, J. R., TATB: The IHE exemplar, Report no. LA-UR-92-3883, Los Alamos National Lab., NM, 1992.

Vanderbilt, D., Soft self-consistent pseudopotentials in a generalized eigenvalue formalism, *Phys. Rev. B: Condens. Matter*, vol. **41**, pp. 7892–7895, 1990.

Vergoten, G., Fleury, G., Blain, M., and Odiot, S., Molecular-structure of aromatic nitro-derivatives. 5. vibration-spectra and analysis by normal coordinate treatment of 1,3,5-triamino-2,4,6-trinitrobenzene, *J. Raman Spectrosc.*, vol. **16**, pp. 143–148, 1985.

VoigtMartin, I. G., Li, G., Yakimanski, A., Schulz, G., and Wolff, J. J., The origin of nonlinear optical activity of 1,3,5-triamino-2,4,6-trinitrobenzene in the solid state: The crystal structure of a non-centrosymmetric polymorph as determined by electron diffraction, *J. Am. Chem. Soc.*, vol. **118**, pp. 12830–12831, 1996.

VoigtMartin, I. G., Li, G., Yakimanski, A. A., Wolff, J. J., and Gross, H., Use of electron diffraction and high-resolution imaging to explain why the non-dipolar 1,3,5-triamino-2,4,6-trinitrobenzene displays strong powder second harmonic generation efficiency, *J. Phys. Chem. A*, vol. **101**, pp. 7265–7276, 1997.

Wentzcovitch, R. M., Invariant molecular-dynamics approach to structural phase-transitions, *Phys. Rev. B: Condens. Matter*, vol. **44**, pp. 2358–2361, 1991.

Wentzcovitch, R. M., Yu, Y. G. G., and Wu, Z. Q., Thermodynamic properties and phase relations in mantle minerals investigated by first principles quasiharmonic theory, *Theor. Comput. Methods Min. Phys.: Geophys. Appl.*, vol. **71**, pp. 59–98, 2010.

Willey, T. M., Hoffman, D. M., van Buuren, T., Lauderbach, L., Gee, R. H., Maiti, A., Overturf, G. E., Fried, L. E., and Ilavsky, J., Changes in pore size distribution upon thermal cycling of TATB-based explosives measured by ultra-small angle x-ray scattering, *Propellants Explos. Pyrotech.*, vol. **34**, pp. 406–414, 2009.

Wu, C. J. and Fried, L. E., Ring closure mediated by intramolecular hydrogen transfer in the decomposition of a push-pull nitroaromatic: TATB, *J. Phys. Chem. A*, vol. **104**, pp. 6447–6452, 2000.

Wu, Z. and Wentzcovitch, R. M., Vibrational and thermodynamic properties of wadsleyite: A density functional study, *J. Geophys. Res.*, vol. **112**, no. B12202, 2007.

Wu, C. J., Yang, L. H., Fried, L. E., Quenneville, J., and Martinez, T. J., Electronic structure of solid 1,3,5-triamino-2,4,6-trinitrobenzene under uniaxial compression: Possible role of pressure-induced metallization in energetic materials, *Phys. Rev. B: Condens. Matter*, vol. **67**, p. 235101, 2003.

Wu, Z. Q., Wentzcovitch, R. M., Umemoto, K., Li, B. S., Hirose, K., and Zheng, J. C., Pressure-volume-temperature relations in MgO: An ultrahigh pressure-temperature scale for planetary sciences applications, *J. Geophys. Res.*, vol. **113**, no. B06204, 2008.

Wu, Z., Kalia, R. K., Nakano, A., and Vashishta, P., Vibrational and thermodynamic properties of β-HMX: A first-principles investigation, *J. Chem. Phys.*, vol. **134**, p. 204509, 2011.

Yetter, R. A., Dryer, F. L., Allen, M. T., and Gatto, J. L., Development of gas-phase reaction-mechanisms for nitramine combustion, *J. Propul. Power*, vol. **11**, pp. 683–697, 1995.

Yu, Y. G. G. and Wentzcovitch, R. M., Density functional study of vibrational and thermodynamic properties of ringwoodite, *J. Geophys. Res.*, vol. **111**, no. B12202, 2006.

Zeman, S., The thermoanalytical study of some aminoderivaties of 1,3,5-trinitrobenzene, *Thermochim. Acta*, vol. **216**, pp. 157–168, 1993.

Zhang, C. Y., Ma, Y., and Jiang, D. J., Charge transfer in TATB and HMX under extreme conditions, *J. Mol. Model.*, vol. **18**, pp. 4831–4841, 2012a.

Zhang, H. B., Li, N., Tian, C. B., Liu, T. F., Du, F. L., Lin, P., Li, Z. H., and Du, S. W., Unusual high thermal stability within a series of novel lanthanide TATB frameworks: Synthesis, structure, and properties (TATB=4,4',4"-s-triazine-2,4,6-triyl-tribenzoate), *Cryst. Growth Des.*, vol. **12**, pp. 670–678, 2012b.

Zhang, L. Z., Zybin, S. V., van Duin, A. C. T., Dasgupta, S., Goddard, W. A., and Kober, E. M., Carbon cluster formation during thermal decomposition of octahydro-1,3,5,7-tetranitro-1,3,5,7-tetrazocine and 1,3,5-triamino-2,4,6-trinitrobenzene high explosives from ReaxFF reactive molecular dynamics simulations, *J. Phys. Chem. A*, vol. **113**, pp. 10619–10640, 2009.

Zhao, J. J. and Liu, H., High-pressure behavior of crystalline FOX-7 by density functional theory calculations, *Comput. Mater. Sci.*, vol. **42**, pp. 698–703, 2008.

Zhu, W. H., Zhang, X. M., Wei, T., and Xiao, H. M., First-principles study of crystalline mono-amino-2,4,6-trinitrobenzene, 1,3-diamino-2,4,6-trinitrobenzene, and 1,3,5-triamino-2,4,6-trinitrobenzene, *J. Mol. Struct. THEOCHEM*, vol. **900**, pp. 84–89, 2009.